Published in final edited form as:
Neuron. 2010 June 10; 66(5): 710–723. doi:10.1016/j.neuron.2010.04.033.

An Arf-like small G protein, ARL-8, promotes the axonal transport of presynaptic cargoes by suppressing vesicle aggregation

Matthew P. Klassen[1,2,6], **Ye E. Wu**[1,6], **Celine I. Maeder**[1], **Isei Nakae**[3], **Juan G. Cueva**[4], **Emily K. Lehrman**[1], **Minoru Tada**[3], **Keiko Gengyo-Ando**[5], **George J. Wang**[1], **Miriam Goodman**[4], **Shohei Mitani**[5], **Kenji Kontani**[3], **Toshiaki Katada**[3], and **Kang Shen**[1,*]

[1]Howard Hughes Medical Institute, Department of Biology, Stanford University, 385 Serra Mall, Stanford, California 94305, USA

[2]Neurosciences Program, Stanford University School of Medicine, 385 Serra Mall, Stanford, California 94305, USA

[3]Department of Physiological Chemistry, University of Tokyo, 7-3-1 Hongo, Bunkyo-ku, Tokyo 113-0033, Japan

[4]Department of Molecular and Cellular Physiology, Stanford University, Stanford, California 94305

[5]Department of Physiology, Tokyo Women's Medical University School of Medicine, 8-1, Kawada-cho, Shinjuku-ku, Tokyo

SUMMARY

Presynaptic assembly requires the packaging of requisite proteins into vesicular cargoes in the cell soma, their long-distance microtubule-dependent transport down the axon and finally, their reconstitution into functional complexes at prespecified sites. Despite the identification of several molecules that contribute to these events, the regulatory mechanisms defining such discrete states remain elusive. We report the characterization of an Arf-like small G protein, ARL-8, required during this process. *arl-8* mutants prematurely accumulate presynaptic cargoes within the proximal axon of several neuronal classes, with a corresponding failure to assemble presynapses distally. This proximal accumulation requires the activity of several molecules known to catalyze presynaptic assembly. Dynamic imaging studies reveal that *arl-8* mutant vesicles exhibit an increased tendency to form immotile aggregates during transport. Together, these results suggest that *arl-8* promotes a trafficking identity for presynaptic cargoes, facilitating their efficient transport by repressing premature self-association.

[*]Correspondence: kangshen@stanford.edu.
[6]These authors contributed equally to this work

AUTHOR CONTRIBUTIONS Matthew P. Klassen identified the mutation for *arl-8(wy271)*. Ye E. Wu and Matthew P. Klassen characterized the mutant phenotype and performed the genetic interaction experiments. Celine I. Maeder performed the dynamic imaging experiments. Emily K. Lehrman isolated the *wy271* mutation. Isei Nakae, Minoru Tada, Toshiaki Katada and Kenji Kontani performed the aldicarb assays and Western blot analysis. Juan G. Cueva, George J. Wang and Miriam Goodman performed the EM analysis. Keiko Gengyo-Ando and Shohei Mitani generated the *arl-8(tm2504)* and *arl-8(tm2388)* alleles. Kang Shen supervised the project. Matthew P. Klassen, Ye E. Wu and Kang Shen wrote the paper.

INTRODUCTION

The polarization of neurons reflects their specialized role in the processing of sensory, cognitive and motor information. Although most clearly reflected in the subdivision of neuronal processes into axon and dendrite, neurons exhibit finer levels of polarization. For example, while axons mediate long-distance communication intracellularly, presynaptic terminals are discretely specified to convey this information selectively to postsynaptic partners. Presynapses are characterized by a pool of synaptic vesicles (SVs) and an active zone, each containing a large assemblage of proteins. Consequently, the specification and assembly of these complexes represent a formidable cellular challenge (Jin and Garner, 2008; Owald and Sigrist, 2009), a coordinated process that remains an enduring question in neuronal cell biology.

Our understanding of how proteins are delivered to the presynaptic terminal began with the observation that microtubules are essential for the anterograde movement of acetylcholinesterase down the axon (Kreutzberg, 1969). It was later discovered that the kinesin-3 family motors mediate the anterograde transport of presynaptic proteins (Hall and Hedgecock, 1991; Okada et al., 1995; Pack-Chung et al., 2007). Electron and light micrographic studies demonstrated that many presynaptic cargoes are transported down the axon in synaptic vesicle precursors (SVPs) (Ahmari et al., 2000; Kraszewski et al., 1995; Matteoli et al., 1992; Tao-Cheng, 2007; Tsukita and Ishikawa, 1980). An additional vesicular subtype, 80 nanometer dense core Piccolo-Bassoon transport vesicles (PTVs), likely represent modular packets that assemble the active zone cytomatrix (Shapira et al., 2003; Zhai et al., 2001). Live imaging in cultured vertebrate neurons also revealed that packets of SVPs travel along axons intermittently and in either direction, occasionally splitting into smaller packets or merging into larger clusters (Ahmari et al., 2000; Dai and Peng, 1996; Kraszewski et al., 1995).

Interestingly, the transition from a trafficking complex to an assembled presynaptic terminal can occur very quickly. Multi-vesicle complexes labeled with GFP-Vamp2/synaptobrevin II can rapidly accumulate at new axodendritic contact sites and become capable of stimulation-evoked SV recycling (Ahmari et al., 2000). Intracellularly, the recruitment of several active zone components, including the scaffolding proteins SYD-2/Liprin-α, SYD-1, ELKS/ERC/CAST and the serine-threonine kinase SAD-1, positively regulate the assembly of the presynaptic apparatus (Crump et al., 2001; Jin and Garner, 2008; Owald and Sigrist, 2009). However, despite our understanding of the regulatory mechanisms that catalyze the assembly state, those that facilitate the microtubule-dependent trafficking and targeting of presynaptic cargoes remain incomplete.

Membrane traffic involves four discrete steps: budding from donor organelles, transport, tethering to target membranes and fusion (Bonifacino and Glick, 2004). Their coordinated processivity is regulated by small GTPases of the Ras superfamily. For example, Arf1/Sar1 GTPases recruit coat complexes to budding membranes (D'Souza-Schorey and Chavrier, 2006). Another Arf family member, Arf6, modulates endosomal plasma membrane trafficking by recruiting a phosphatidylinositol 5-kinase (Aikawa and Martin, 2003; Krauss et al., 2003). Subsequent to directed transport, another subclass of the Ras superfamily, the Rab GTPases, act as essential regulators of vesicle-tether recognition at target membranes (Cai et al., 2007). However, although several Ras family GTPases associate with synaptic vesicles (Burre and Volknandt, 2007), none are known to regulate precursor vesicle transport or insertion. The SV-associated Rab GTPase Rab3 has been implicated in Ca^{2+}-mediated exocytosis (Nonet et al., 1997; Schluter et al., 2004) and more recently in regulating the composition of presynaptic active zones (Graf et al., 2009). In addition to the classic Arf family members, genomic sequencing has identified a number of well conserved

Arf-like small G proteins (Arls), but the functions of most are not well understood (Gillingham and Munro, 2007).

In a forward genetic screen for genes that regulate presynaptic patterning in the *C. elegans* motoneuron DA9, we isolated a strong loss-of-function mutant in the Arf-like small G protein *arl-8*. *arl-8* mutants prematurely accumulate presynaptic cargoes in the proximal axon and concomitantly fail to properly assemble presynapses in distal segments. Dynamic imaging reveals that synaptic vesicle precursors form aggregates along the transport route that cannot be efficiently remobilized. We therefore propose that *arl-8* facilitates the trafficking of presynaptic cargo complexes by repressing excessive self-association during axonal transport.

RESULTS

wy271 Mutants Display Strong Proximodistal Defects in the Subcellular Localization of Synaptic Vesicle Proteins

The *C. elegans* cholinergic motoneuron DA9 represents an accessible model to investigate the molecular mechanisms regulating neuronal polarization and synaptic assembly *in vivo*. The DA9 soma resides in the preanal ganglion, where it extends a molecularly and functionally distinct dendrite and axon, the latter forming approximately 25 *en passant* presynapses within a discrete and stereotyped location along the dorsal nerve cord (Figure 1A, Klassen and Shen, 2007; White et al., 1976). To understand the molecular determinants that regulate DA9 presynaptic patterning, we performed an unbiased forward genetic screen, isolating a recessive mutation, *wy271*, which results in a completely penetrant abnormal distribution of the synaptic vesicle marker GFP::RAB-3 in DA9 (compare Figures 1B and 1C). *wy271* animals are temperature-sensitive embryonic/early-larval lethal and slow growing, with synaptic defects evident even at the permissive temperature for growth.

Two key aspects of the *wy271* phenotype are readily observed: a systematic shift of RAB-3 signal towards the proximal axon and the appearance of abnormally large puncta within this region (compare Figures 1B and 1C, quantified in 1E, primary data in Figures 8A and 8D). *wy271* animals also have 30% fewer presynaptic puncta (27.3 +/− 1.6 in *wild type* vs. 17.4 +/− 2.4 in *w271*, $p<0.0001$, SEM, t test, n=20 animals), with the ectopic proximal *wy271* puncta (0–25 μm from commissure) being significantly larger than those observed distally in the putative wild-type synaptic region (>25 μm from commissure) of either genotype (2.07 +/− 0.56 μm^2 in *wy271* 0–25 μm proximal domain vs. 1.28 +/− 0.12 μm^2 in *wild type* and 1.03 +/− 0.23 μm^2 in *wy271* distal domains, $p<0.0001$, SEM, t test, n=95–531 puncta).

To determine whether the *wy271* phenotype manifests itself more broadly within the *C. elegans* nervous system, we examined the presynapses of several other neuronal classes. DB7 is a cholinergic motoneuron whose presynapses reside within a similar anteroposterior domain as DA9 but with opposite proximodistal polarity (Figure 1F). The DB7 phenotype revealed that *wy271* represents a proximodistal rather than anteroposterior positioning defect, with mutant animals accumulating large puncta within proximal axonal segment at the expense of distal puncta (compare Figures 1G and 1H). We also examined GABAergic neurons, notably motoneurons of the D-class (Hallam and Jin, 1998). Subsequent to early-larval metamorphosis, DD neurons form presynapses in a tiled array along the dorsal cord (Figures 1I and 1J). In *wy271* animals, DD neurons fail to form presynapses in distal regions of their normal synaptic domain, leaving gaps between adjacent DD presynaptic regions (compare Figures 1J and 1K). Similarly, in the head interneuron RIA, mCherry::RAB-3 puncta ectopically accumulate in the proximal segment of the RIA process, a region that is exclusively dendritic in wild-type animals (*wyIs93*, data not shown, Margeta et al., 2009). We conclude that SV proteins in several neuronal classes fail to reach their normal location

in the distal axon in *wy271* mutants and instead accumulate into large aggregates proximally.

The Mislocalization of Synaptic Vesicle Proteins in *wy271* Mutants Does Not Appear to Arise From Defects in the Sorting of Vesicular Cargoes or the Specificity of Synaptic Partner Choices

To determine whether the mislocalization of the SV-associated protein RAB-3 represents an ectopic accumulation of SVPs or alternatively the mislocalization or mis-sorting of select presynaptic markers, we examined the localization of two integral membrane synaptic vesicle proteins: synaptobrevin (SNB-1) and synaptogyrin (SNG-1). *arl-8* does not appear necessary for appropriate sorting of vesicular cargoes as all SV markers examined displayed similar defects in their localization (Figure S1). Furthermore, the trafficking of these SV proteins remain dependent on the anterograde kinesin *unc-104*; GFP::RAB-3 mislocalizes within the soma and dendrite in *arl-8; unc-104* double mutants, as in *unc-104* single mutants, suggesting that motor-cargo binding specificity is maintained (*wyIs85*, data not shown).

To further characterize *wy271* mutants, we performed correlative electron microscopy (EM), sectioning through ectopic RAB-3 puncta in the dorsal proximal axon. This analysis revealed large clusters of clear core vesicles, with occasional dense core vesicles and electron dense structures (Figures 2A and 2B). Interestingly, although 28.2% of *arl-8* clear core vesicles had a diameter identical to SVs in wild-type animals (34.68 +/− 3.36 nm in *wild type*, SEM), the majority of mutant vesicles had an increased diameter that distributed around 55 nm (Figure 2C). Increased SV size has been observed in mutants with defects in SV endocytosis (Fergestad et al., 1999; Marza et al., 2008; Nonet et al., 1999; Zhang et al., 1998). To test whether increased SV size and/or defective SV recycling could contribute to the proximal shift of SVs in *wy271* mutants, we examined the localization of RAB-3 and SNB-1 in DA9 in hypomorphic or null mutants of *unc-26/synaptojanin*, *unc-57/endophilin* and *fat-3*, which exhibit defective SV endocytosis and/or increased SV size (Harris et al., 2000; Marza et al., 2008; Schuske et al., 2003). However, none of these mutants phenocopied *wy271* (*wyIs85* and *wyIs92*, data not shown), suggesting that the mislocalization of SVs in *wy271* mutants is not a direct result of increased SV size or impaired SV recycling.

Consistent with the presence of electron dense structures near ectopic vesicle pools in our EM analysis, the active zone markers SYD-2 (Liprin-α, Figure S2) and CCB-1 (β-subunit of voltage-gated calcium channels, *wyEx771*, data not shown) colocalized with ectopic RAB-3 puncta in *wy271* mutants. We also examined endocytic markers, including RAB-5, RAB-7 and RAB-11, which label early, late and recycling endosomes, respectively, previously shown to colocalize with RAB-3 in the D-type GABAergic motoneurons (Brown et al., 2009). These markers exhibited colocalization with RAB-3 in DA9 in wild-type animals and similarly colocalized with ectopic RAB-3 puncta in *wy271* mutants (*wyEx3676*, *wyEx3677* and *wyEx3688*, data not shown). Together, these results suggest a systematic proximal shift of presynaptic components in *wy271* mutants.

The apparent defects in the distribution of SVs may represent an abnormal synaptic partner choice or an inability to respond to the positional information encoded by Wnt-Frizzled signaling (Klassen and Shen, 2007). We therefore examined whether the postsynaptic acetylcholine receptor ACR-16 colocalizes with ectopic RAB-3 puncta in *wy271* mutants. Only 30% of ectopic mCherry::RAB-3 puncta were apposed by strong accumulations of muscle ACR-16::GFP compared to 68% in the Wnt mutant *lin-44(n1792)* (*wyEx802*, n=74–87 puncta, data not shown). Similarly, we failed to observe postsynaptic muscle arms contacting the proximal ectopic presynaptic specializations of *wy271* mutants in our EM

analysis (data not shown). These results suggest that the ectopic SV protein accumulations observed in *wy271* mutants do not represent a direct remapping of synaptic specificity.

wy271 is a Strong Hypomorphic Allele of the Arf-like Small G protein *arl-8* and Functions Cell Autonomously in DA9

Using SNP-SNIP mapping and transgenic rescue, we isolated the genetic lesion of *wy271* to a single open reading frame (*wyEx2317*, data not shown). This single ORF encodes a conserved Arf-like small G protein, *arl-8*, of which *wy271* represents a 247-nucleotide deletion of proximal 5' regulatory sequences, the SL1 splice acceptor and the first 7 nucleotides of the *arl-8* cDNA (Figures 3A and 3B). A putative in-frame alternate start site is encoded by the fourth amino acid (Figure 3B). Arf-family small G proteins display a guanine nucleotide-binding regulated conformational switch, with the GTP-bound state representing an active form that associates with target membranes (Pasqualato et al., 2002).

Several lines of evidence suggest that *wy271* represents a strong reduction of function allele of *arl-8*. Western blotting revealed a strong decrease in ARL-8 protein level in *arl-8(wy271)* mutants (Figure 3C). Furthermore, double-stranded RNA interference of *arl-8* and two additional deletion alleles *tm2504* and *tm2388* (Figure 3A) phenocopy *wy271* (Figures 3D–H and data not shown). The *tm2504* allele eliminates the well-conserved G5 region important for binding to phosphate/Mg^{2+} and the guanine base (Okai et al., 2004; Paduch et al., 2001) and causes a severe maternal embryonic lethality phenotype. Therefore *tm2504* is likely to be a strong loss-of-function or null allele. Since *tm2504* showed a phenotype indistinguishable from that of *wy271*, *wy271* likely represents a strong reduction-of-function allele. ARL-8 displays strong sequence identity across phylogeny, suggesting its function may be highly conserved in most eukaryotes (Figure 3I). Previous research has implicated the vertebrate *arl-8* orthologs in lysosomal trafficking and chromosome segregation, both of which represent microtubule-dependent processes (Bagshaw et al., 2006; Hofmann and Munro, 2006; Okai et al., 2004).

Previous analysis suggests that *arl-8* is expressed in a variety of tissues, including the DA class of motoneurons (Fox et al., 2005; Hunt-Newbury et al., 2007). To determine in which cell(s) *arl-8* is required to rescue the *wy271* DA9 synaptic vesicle phenotype, we expressed the *arl-8* cDNA under the control of a variety of cell and tissue restricted promoters. Expression in postsynaptic muscles using a fragment of the *unc-129* promoter failed to rescue the DA9 phenotype (*wyEx3302*, n=108 animals). However, expression using the *Pitr-1 pB* or *Pmig-13* promoter, which we use to label DA9, robustly rescued the DA9 presynaptic phenotype, suggesting that *arl-8* functions cell-autonomously (*wyEx2342* and *wyEx2337*; strong rescue in 88/99 and 102/113 animals, respectively). Consistent with a conserved function of ARL-8 across phylogeny, expression of human *ARL8A* from the *Pitr-1pB* promoter also rescued the DA9 presynaptic phenotype (*wyEx3454*, strong rescue in 96/98 animals). In agreement with a requirement for GTP binding in ARL-8 activity, expression of a putative constitutively GTP-bound mutant (ARL-8 Q75L) but not a nucleotide-unbound mutant (ARL-8 T34N) in DA9 led to significant rescue of the *wy271* phenotype (Figure S3A).

The observed defects in cholinergic motoneuron synaptic organization led us to examine whether the function of these neurons is also affected. Indeed, *arl-8(tm2388)* and *arl-8(wy271)* mutants exhibit resistance to the acetylcholinesterase inhibitor aldicarb, a phenotype indicative of defects in cholinergic synaptic transmission (Figures 4 and 8) and consistent with our observation that ectopic presynaptic specializations in *arl-8* mutants largely fail to associate with postsynaptic receptors. This phenotype can be rescued by expression of *arl-8* pan-neuronally using the *PF25B3.3* promoter or in cholinergic motoneurons using the *Pacr-2* promoter (Figure 4), corroborating a neuronal locus.

arl-8 Mutants Do Not Perturb the Long-Distance Anterograde Trafficking of Non-Synaptic Proteins or the Localization of Dendritic Markers

Arf-family small G proteins are diverse regulators of membrane traffic and cytoskeletal organization (Gillingham and Munro, 2007). To determine whether *arl-8* specifically regulates aspects of presynaptic development or, conversely, is a more pleitropic regulator of cellular growth and polarization, we examined several general aspects of neuronal structure and polarity. DA9 and DB7 motoneuron axons extend long asynaptic segments distally and their morphology and stereotyped termination points are maintained in *arl-8* mutants (*wyEx1902* and *wyEx1199*, data not shown). We also examined the targeting of non-synaptic cargoes and organelles. Mitochondria, labeled using the membrane-targeting domain of the outer membrane translocase TOM20 (Hulett et al., 2008), successfully trafficked throughout the axon and dendrite in *arl-8* mutants (Figures S5A–D). Furthermore, the transmembrane innexin subunit INX-10 remains localized in punctate structures throughout the axon and dendrite (Figures S5E and S5F). Lastly, the plus-end directed kinesins UNC-104/KIF1A (Figures S5G and S5H) and UNC-116/KIF5 (*wyEx3119*, data not shown) maintain their characteristic accumulation at the distal tip of the DA9 axon.

We also considered the possibility that a defective segregation of axonal and dendritic polarity could underlie the presynaptic targeting defects. While *arl-8* mutants do not display ectopic accumulations of presynaptic proteins in the dendrite in DA9, we nonetheless examined the localization of several somatodendritically targeted proteins to determine whether dendritic polarity and fate were appropriately restricted. A member of the minus-end directed kinesin-13 family, KLP-16/KIFC3, localizes asymmetrically within the somatodendritic domain of DA9 in both wild-type and mutant animals, consistent with a minus-end-out or mixed polarity of microtubules within the DA9 dendrite (Figures S6A and S6B). Furthermore, the somatodendritic localization of CAM-1/Ror receptor tyrosine kinase, DYS-1b/Dystrophin and F35D2.3/Fibrillin remain unaffected (Figures S6C–H, Sieburth et al., 2005). We conclude that the appropriate segregation of axonal and dendritic polarity is maintained in *arl-8* mutants.

The Mislocalization of Synaptic Vesicles in *arl-8* Mutants is Unlikely to Arise From Deficits in Lysosome Biogenesis or Function

Given previous findings that human and *Drosophila* ARL8 othologs affect lysosome motility in cell culture (Bagshaw et al., 2006; Hofmann and Munro, 2006) and furthermore that lysosomes and synaptic vesicles can both be generated from endosomes (Bonanomi et al., 2006; Mullins and Bonifacino, 2001; Newell-Litwa et al., 2007), we explored the possibility that the *arl-8* presynaptic phenotype might result from the mis-sorting of lysosomal proteins or defects in lysosome function. However, in both *wild type* and *arl-8* animals, the localization of a lysosomal transmembrane protein, LMP-1::YFP (Kostich et al., 2000; Treusch et al., 2004), is largely restricted to the perikaryon and only shows weak fluorescence in the dendrite and the axon (Figures S4A and S4B), suggesting that lysosome-targeted proteins do not sort ectopically into presynaptic cargoes in *arl-8* mutants.

We also examined a potential role for the heterotetrameric AP3 adaptor complex, which has been implicated in protein sorting from endosomes into lysosomes and SVs (Bonanomi et al., 2006; Newell-Litwa et al., 2007). Double-stranded RNA interference against the *C. elegans* genes encoding the β3, δ3 and μ3 subunits, *apb-3*, *apd-3* and *apm-3*, respectively, did not cause an ectopic accumulation of presynaptic cargoes within the proximal axon, although we did observe a slight accumulation of SNB-1::YFP within the cell soma (*wyIs92*, data not shown). Similarly, *apb-3(ok429)*, a putative null deletion allele which causes loss of lysosome-related gut granules (Hermann et al., 2005), did not phenocopy *arl-8*, although we did observe weak dendritic accumulation of GFP::RAB-3 (compare Figures S4C and S4D).

Finally, *cup-5(ar465)* mutants, which show severe lysosome biogenesis defects (Treusch et al., 2004), retain a wild-type distribution of GFP::RAB-3 in DA9 (compare Figures S4C and S4E). We conclude that the effect of *arl-8* on the localization of SVs is unlikely to reflect a function dependent upon lysosome biogenesis or activity.

ARL-8 Associates with Presynaptic Cargoes and Likely Regulates Vesicular Transport in Axons

We next considered potential roles for ARL-8 in regulating the axonal trafficking of synaptic vesicle precursors. The subcellular localizations of Arf small G proteins correlate with their diverse roles in regulating membrane trafficking and cytoskeletal organization (Gillingham and Munro, 2007). To understand where ARL-8 might function, we expressed a functional ARL-8::YFP fusion protein specifically in DA9. ARL-8::YFP is strongly enriched at presynaptic terminals in DA9, where it colocalizes with mCherry::RAB-3 (Figure 5). This enrichment at the presynapse requires the synaptic vesicle precursor kinesin *unc-104*; ARL-8::YFP is absent from the presynaptic terminal, but instead colocalizes with mCherry::RAB-3 in the cell body and dendrite in *unc-104* mutants *(wyEx3198*, data not shown). To examine whether ARL-8 is present on transporting SVPs, we imaged the proximal segment of ARL-8::YFP expressing DA9 axons using a highly sensitive CCD camera. Time-lapse imaging revealed that dim ARL-8::YFP puncta move rapidly in both anterograde and retrograde directions, similar to the movements of GFP::RAB-3 labeled vesicles (Movie S1). Indeed, we observed co-movements of ARL-8::YFP and mCherry::RAB-3 puncta (Movie S2). These results are consistent with previous identification of ARL-8 orthologs within a SV fraction purified from rat brain (Takamori et al., 2006).

In accordance with a requirement for GTP binding in the membrane targeting of ARL-8, the putative nucleotide-unbound mutant ARL-8 T34N::YFP appeared diffuse and exhibited no enrichment at the presynapses in DA9 (Figures S3E–G). Unexpectedly, the putative GTP-locked mutant ARL-8 Q75L::YFP also displayed little enrichment at the DA9 presynapses although it did appear to bind to other membranous structures within the cell body (Figures S3B–D). The regulated conformational switch of Arf-family small G proteins is thought to act as a coincidence detector for target membrane and guanine exchange factor activity (Pasqualato et al., 2002). Accordingly, the constitutive GTP-bound form may interfere with such target-specific activation, leading to non-selective binding to other membranous structures, which may explain the lower rescuing activity of the mutant compared to wild-type ARL-8 when expressed at similar levels (Figure S3A).

The putative localization of ARL-8 on trafficking and mature SVs raised the possibility that it functions to regulate their transport. We therefore attempted to rescue the *arl-8* mutant phenotype by overexpressing the appropriate anterograde motors. We have confirmed previous observations (Hall and Hedgecock, 1991) that the kinesin UNC-104/KIF1A is the critical motor for anterogradely transporting SVs and active zone proteins in the DA9 neuron. In *unc-104* mutants, RAB-3 and the active zone protein SYD-2 are completely absent from the axon and instead mislocalize within the cell body and dendrite (Figure S7). We therefore created transgenic *arl-8* mutant animals overexpressing *unc-104* in DA9 to determine whether we could bypass the requirement of *arl-8* in the proper localization of SVs. Surprisingly, overexpression of *unc-104* in DA9 robustly suppressed the mislocalization of RAB-3 in *arl-8* mutants (quantified in Figure 1E, n=20 animals), with nearly 35% of animals appearing qualitatively indistinguishable from wild-type animals (example in Figure 1D, n=106 animals). This result argues strongly that overproduction of the UNC-104 motor is sufficient to compensate for the effect of loss of ARL-8 with respect to SV localization, suggesting that the *arl-8* mutants display insufficient anterograde transport.

Dynamic Imaging Reveals that Self-Reinforcing Aggregation of Synaptic Vesicle Precursors May Underlie the *arl-8* Mutant Phenotype

To evaluate potential microscale changes in SVP transport, we performed time-lapse imaging of trafficking presynaptic cargoes in DA9 *in vivo*. Small mobile and stable (over the imaging session) GFP::RAB-3 puncta can be readily visualized in asynaptic axonal regions using a high-sensitivity CCD camera. Importantly, the presence and anterograde velocity of these small puncta are strongly *unc-104*-dependent, suggesting that they likely represent trafficking presynaptic cargoes (C. Maeder and K. Shen, unpublished data). We focused on the axon initial segment emanating posteriorly from the cell soma (red box in Figure 6A), normalizing all data by time and length of the imaged axonal segment.

Within this subcellular compartment of DA9, moving GFP::RAB-3 particles trafficked distally in the anterograde direction in 68% of observed events and retrogradely towards the cell soma in 32% of observed events, a ratio not significantly different between *wild type* and *arl-8* animals (Figure 6B left). Moreover, the velocity of anterograde and retrograde movements were both statistically indistinguishable between genotypes (Figure 6B right). Similar results were observed for the distal asynaptic axon (DAA, green box in Figure 6A, data not shown). In stark contrast however, we observed a 45% reduction in the incidence of moving particles and an increase in the number and size of stable particles in the *arl-8* ventral axon (Figures 6A and 6C). The reduced incidence of moving puncta was even more pronounced in the distal asynaptic axon (Figure 6D). To explore potential relationships between the intensity of RAB-3 puncta and their tendencies to move, we plotted the intensity distribution of puncta that are stable, anterogradely, or retrogradely trafficked in both *wild type* and *arl-8* mutant animals. In wild-type animals, stable and moving puncta are distributed in a virtually non-overlapping fashion, with moving puncta being considerably dimmer, a pattern that persists in *arl-8* mutants (Figure 7A). However, the intensities of stable puncta are dramatically increased in *arl-8* mutants, with only a mild increase in the intensities of moving particles (Figure 7A).

The correlated reduction in moving particles and the increased number and intensity of stable particles in *arl-8* mutants led us to examine potential kinetic interactions between these populations. We separated the puncta into three groups: puncta from wild-type animals (*wt*), *arl-8* puncta with fluorescence intensity comparable to that of *wild type* puncta (dim *arl-8*) and *arl-8* puncta with intensity greater than that of the brightest *wild type* puncta (bright *arl-8*). To understand how these aggregates might form in the axon, we first documented whether each moving particle in our data set would stop or continue upon encountering a stable particle in its path. Such analysis revealed that, while there was no difference in the stalling probability for moving puncta encountering the *wt* and dim *arl-8* groups, moving puncta encountering the bright *arl-8* group displayed a greater than two-fold increase in stalling probability (Figure 7B left). Second, we measured the frequency that a stable punctum would give rise to a mobile punctum. We found that the dissociation rate for the dim *arl-8* group was significantly lower compared to puncta of similar intensity in wild-type animals (Figure 7B right). Taken together, these measurements suggest that the tendency of trafficking vesicles to aggregate is higher and self-reinforcing in *arl-8* mutants, initially due to a reduced dissociation rate for dim stable puncta and subsequently the result of an enhanced aggregation tendency for moving particles encountering bright stable puncta.

Ectopic Synaptic Vesicle Precursor Aggregation Requires the Activity of Several Presynaptic Assembly Molecules

Our dynamic imaging results could be explained by two potential mechanisms. First, aggregates of trafficking SVPs in *arl-8* mutants may reflect abnormalities in the function of molecular motors or microtubules. Alternatively, trafficking cargoes may possess an

enhanced capacity to self-associate in *arl-8* mutants, resulting in cargo complexes too large for effective anterograde transport. Our dynamic analysis of moving puncta reveals that the run length and speed for both anterograde and retrograde movements in *arl-8* mutants are unaffected (Figure 6B and data not shown), suggesting that normally sized cargoes are effectively transported in the absence of interactions with stable puncta. To determine whether vesicle aggregation in *wy271* mutants requires an adhesive activity, we constructed double mutants between *arl-8(wy271)* and known positive regulators of SV clustering, surmising that these molecules might also promote vesicle clustering during transport. If reducing endogenous assembly forces suppressed aggregation in *arl-8* mutants, it would suggest that the *arl-8* defect is principally one of inappropriate self-association between cargoes rather than an inability to transport normal cargoes effectively.

As previously reported in other neurons (Crump et al., 2001; Dai et al., 2006; Patel et al., 2006; Zhen and Jin, 1999), *syd-2*/liprin-α, *syd-1* and the serine threonine kinase *sad-1* represent important contributors to DA9 presynaptic assembly. Assembly phenotypes in DA9 reflect a fragmentation and dispersal of SV clusters throughout the neuron (compare Figures 8A–C, quantified in Figures 8G and 8H, data not shown for *syd-1*). Strikingly, *arl-8; sad-1, arl-8; syd-2, and arl-8; syd-1* double mutants all strongly but incompletely suppress the proximodistal SV distribution defect observed in *arl-8* single mutants, with significant amounts of GFP::RAB-3 now distributed distally within the axon (compare Figures 8D–F, quantified in Figures 8G and 8H, n=20 animals, data not shown for *arl-8; syd-1*). Additionally, although similar numbers of ectopic puncta were still observed within the proximal 25 μm of the dorsal axon, the enlarged size of these puncta observed in *arl-8* mutants was also strongly suppressed (2.07 +/− 0.56, 0.89 +/− 0.16 and 0.98 +/− 0.18 μm^2 in *arl-8(wy271)* alone, *sad-1(ky330); arl-8(wy271)* and *syd-2(wy5); arl-8(wy271)*, respectively. SEM, $p<0.001$, t test, n=82–125 puncta). Furthermore, *sad-1* and *syd-2* mutants also significantly suppressed the aldicarb resistance phenotype of *arl-8* mutants (Figures 8I–J). Together, these results suggest that *arl-8* and the assembly molecules *sad-1*, *syd-1* and *syd-2* antagonistically regulate the intrinsic self-association activity of presynaptic cargoes. Because it is well established that *syd-2* and *sad-1* also function at the presynaptic terminals to cluster synaptic vesicles, our model predicts that overactivation of *arl-8* may inhibit SV clustering at presynaptic terminals. Indeed, overexpression of *arl-8* in DA9 significantly decreased the fluorescence intensity of presynaptic RAB-3 puncta (3253.79 +/− 174.62 units in *wild type* vs. 1815.06 +/− 85.26 units in *arl-8* overexpressing animals, compare Figures 8K and 8L, quantified in Figure 8M).

DISCUSSION

The coordinated transport of presynaptic proteins and their precise assembly at specific sites within the axon represents an exquisite example of subcellular polarization. The Arf-like small G protein *arl-8* may be a critical regulator of this process. Strong reduction-of-function mutants of *arl-8* prematurely accumulate presynaptic machinery within the proximal axons of several neuronal classes, with corresponding deficits in the distal axon. Dynamic imaging and the strong genetic interactions with the presynaptic assembly molecules *syd-2*/*liprin*-α, *sad-1* and *syd-1* further suggest that *arl-8* may repress the excessive self-association of trafficking presynaptic cargoes.

ARL-8 Promotes a Discrete Trafficking Identity for Presynaptic Cargoes

It is well accepted that synaptic vesicle precursors are transported along microtubule tracks. However, little is known about the regulatory mechanisms that facilitate their transport. Interestingly, in cultured neurons many SVPs appear to move as coherent clusters not stably anchored to the cell surface. Moreover, these clusters can dynamically fragment into smaller units or coalesce into larger ones (Ahmari et al., 2000; Dai and Peng, 1996; Kraszewski et

al., 1995). These findings suggest that trafficking precursors may represent a discrete state for presynaptic cargoes, which possess an intrinsic aggregation propensity independent of cell-cell interactions between synaptic partners. Consistent with these observations, our *in vivo* dynamic imaging experiments reveal that GFP::RAB-3 puncta in DA9 axon exhibit a wide range of intensities (Figure 7A), likely representing clusters of different numbers of SVPs. We also observed a strong correlation between puncta intensity and motility, with the dimmer puncta showing a higher tendency to move.

Our findings suggest that ARL-8 is critical for promoting a trafficking identity for presynaptic cargoes. Loss-of-function mutants of *arl-8* display an inability to deliver presynaptic components into the distal axon. Furthermore, dynamic imaging reveals a dramatic reduction in the number of motile GFP::RAB-3 puncta along the transport route, with a corresponding increase in the number of large stable puncta. The end phenotype observed in *arl-8* mutants likely reflects a two-stage process. The initial driving force for aggregate formation appears to result from the reduced dissociation of small stable puncta in *arl-8* mutants. Subsequently, these aggregates achieve a critical mass capable of precipitating further aggregation, perhaps by interacting with multiple microtubule tracks. Accordingly, one model that conceptualizes these findings is that SVPs possess an intrinsic self-adhesive capacity that must be suppressed by ARL-8 during transport in order to facilitate the effective trafficking of small clusters down the axon (Figure S8).

Presynaptic Assembly May Represent a Process Intrinsic to Trafficking Precursors

If trafficking synaptic vesicles move in clusters, what are the forces that hold them together? At developing presynapses, several active zone proteins including SYD-2/Liprin-α, ELKS/Bruchpilot, SAD-1/SAD kinase, SYD-1 and piccolo/bassoon, play important roles in the clustering of presynaptic proteins and vesicles (Crump et al., 2001; Jin and Garner, 2008; Owald and Sigrist, 2009). Our genetic interaction data argues that SAD-1, SYD-2 and SYD-1 may also promote vesicle clustering during transport; loss-of-function mutants in these three genes significantly suppress the *arl-8* phenotype. This genetic interaction is unexpected because active zone proteins are thought to be packaged into and trafficked as dense core vesicles (PTVs), a vesicle population distinct from clear core SVPs both biochemically and ultrastructurally (Shapira et al., 2003; Zhai et al., 2001). However, recent EM analysis of trafficking presynaptic cargoes revealed that PTVs carrying piccolo and bassoon associate with clear core SVPs during axonal transport, providing an ultrastructural basis for potential interactions between these two vesicular subtypes (Tao-Cheng, 2007). Furthermore, work in *Drosophila* suggests that Liprin-α is necessary for the efficient transport of presynaptic cargoes (Miller et al., 2005). Finally, observations that multi-SVP complexes can rapidly accumulate at new axodendritic contact sites and become capable of stimulation-evoked SV recycling (Ahmari et al., 2000) also corroborate a close spatiotemporal relationship during transport. Accordingly, it is conceivable that the active zone proteins responsible for presynaptic assembly trigger the association of SVPs during axonal trafficking, with ARL-8 representing an antagonistic force to control the degree of aggregation.

A Conserved Role for ARL-8 in Microtubule-Dependent Vesicular Transport

The observation that ARL-8 exhibits a high degree of sequence conservation across phylogeny suggests it may function similarly in most eukaryotes, a hypothesis that is supported by the rescuing activity of the human ARL8A ortholog in *C. elegans*. Indeed, proteomic analysis of vertebrate synaptic vesicles identified ARL8 orthologs as SV-associated proteins (Takamori et al., 2006). Hence, it is conceivable that ARL8 also plays an important role in regulating axonal transport of SVPs in the vertebrate nervous system.

While the cellular functions of ARL-8 are only starting to be realized, existing publications suggest that it is involved in diverse cellular processes related to the microtubule-dependent transport of intracellular organelles. Okai and colleagues found that expression of dominant negative GIE1 (also known as ARL8A), one of the two human orthologs of ARL-8, or knocking down GIE1 with RNAi, causes abnormalities in chromosome segregation (Okai et al., 2004), a process which requires the coordinated regulation of microtubule dynamics and a number of molecular motors. Furthermore, two independent labs have demonstrated that ARL8A/B localize to lysosomes and cells overexpressing ARL8A or ARL8B redistribute lysosomes distally towards the plasma membrane (Bagshaw et al., 2006; Hofmann and Munro, 2006). Time-lapse imaging experiments revealed that overexpression of ARL8A or ARL8B cause lysosomes to move more frequently and over greater distances.

It is interesting to compare the *ARL8* gain-of-function phenotype for lysosome targeting with the loss-of-function phenotype in the present study. In both systems, the directionality of organelle movements is not affected. However, activation of ARL8 seems to promote microtubule-mediated trafficking while loss of ARL-8 reduces trafficking. Based upon our dynamic imaging analysis, this trafficking defect may arise from the formation of abnormally large vesicular complexes (Figure 7). It will be interesting to test if the size of moving lysosome complexes is also regulated by ARL-8 as it is conceivable that ARL-8 has a general function in regulating the size of trafficking complexes during microtubule-based transport. Alternatively, ARL-8 might regulate the precise composition or size of organelle precursors, which in turn facilitates their trafficking. Future identification of upstream regulators and downstream effectors of ARL-8 may help differentiate these possibilities.

EXPERIMENTAL PROCEDURES

Strains and Genetics

Worms were raised on OP50 *E. coli* seeded NGM plates at 20°C, excepting for the dynamic imaging experiments as detailed below. The mutant strains CB406 *unc-57(e406)I*, CB1265 *unc-104(e1265)II*, CZ1893 *syd-1(ju82)II*, BX30 *fat-3(wa22)IV* and DR97 *unc-26(e345)IV* were obtained through the *Caenorhabditis* Genetics Center and *arl-8(tm2504)IV* / *nT1[qIs51] (IV;V)* and *arl-8(tm2388)IV* through the National Bioresource Project (Japan). *fat-3(lg8101)IV* was kindly provided by G. Lesa, *sad-1(ky330)X* by C. I. Bargmann, *syd-2(wy5)X* by D. Chao and *juIs1* (*Punc-25::snb-1::gfp*) by Y. Jin. N2 Bristol was utilized as the wild-type reference strain.

Genetic Screen and SNP mapping

The *wy271* allele was isolated from an F2 semiclonal screen of 3,000 haploid genomes in the strain *wyIs109*. Worms were mutagenized with 50 mM EMS. SNIP-SNP mapping, rescue and sequencing were performed using standard protocols.

Cloning and Constructs

Expression clones were made in the pSM vector, a derivative of pPD49.26 (A. Fire) with extra cloning sites (S. McCarroll and C. I. Bargmann, personal communication), or the pFX vector. The following plasmids and strains were generated as previously described: wyIs85 (Pitr-1 pB::gfp::rab-3), wyIs92 (Pmig-13::snb-1::yfp), wyIs93 (Pglr-3::mCherry::rab-3, Pglr-3::glr-1::gfp), wyIs109 (Pmig-13::cfp::rab-3, Pmig-13::snb-1::yfp, Pmig-13::sng-1::mcherry), wyEx403 (Pitr-1 pB::cam-1::yfp), wyEx771 (Pmig-13::gfp::ccb-1, Pmig-13::mCherry::rab-3), wyEx802 (Pmyo-3::acr-16::gfp, Pmig-13::mCherry::rab-3), wyEx1199 (Punc-$129_{\text{DB neuron}}$::gfp::rab-3), wyEx1902 (Pitr-1 pB::mCherry), wyEx2055 (Pitr-1 pB::gfp::syd-2, Pitr-1 pB::mCherry::rab-3), wyEx2396 (Pitr-1 pB::F35D2.3/ fibrillin::yfp) (Klassen and Shen, 2007; Margeta et al., 2009; Poon et al., 2008). Other

transgenic strains were generated using standard techniques as detailed in Supplemental Experimental Procedures.

Fluorescence Confocal Imaging and Quantification

Images of fluorescently tagged fusion proteins were captured in live *C. elegans* using a Plan-Apochromat 63×1.4 or 40×1.3 objective on a Zeiss LSM710 confocal microscope. Worms were immobilized using a mixture of 225 mM 2,3-butanedione monoxime (Sigma) and 2.5 mM levamisole (Sigma) in 10 mM Na HEPES.

Confocal montages of DA9 dorsal cords were assembled by imaging 20 young adult hermaphrodites of similar size using identical image and laser settings for each genotype. Straightened dorsal cords were extracted from these images using the `straighten to line function' in the EMBL suite of ImageJ. These images were then aligned in register along the anteroposterior axis using the DA9 commissure as a landmark.

For quantifying the mean GFP::RAB-3 intensity along these dorsal cords, background fluorescence was first subtracted by calculating the average intensity of each image in a proximal region devoid of GFP::RAB-3 puncta. Mean intensity graphs were then generated using the `plot profile' function or by defining a 25 μm region of interest (ROI) and calculating the mean intensity for each animal within that ROI. Puncta number and size were calculated using the `analyze particles' function, using an intensity threshold of 20 and a puncta size threshold of 3 pixels.

Correlative Light and Electron Microscopy (CLEM)

Young adult worms were agarose embedded, imaged with fluorescence and DIC microscopy, high-pressure frozen, and freeze substituted as described (Kolotuev et al., 2010). For sectioning, the fluorescent RAB-3 puncta were located based on their distance from the anus with the assistance of laser carving.

Serial, 50 nm thin sections were cut with a diamond knife on a Leica Ultracut S microtome and collected on Formvar-coated slot grids. To enhance contrast, sections were poststained in 3.5% uranyl acetate for 30 seconds and Reynold's lead citrate preparation for 3 minutes. The grids were imaged on a Jeol TEM 1230 transmission electron microscope (Tokyo, Japan) and images acquired with a Gatan 967 slow-scan, cooled CCD camera (Pleasanton, CA). ImageJ was used to count and measure the diameter of vesicles.

ARL-8 antibody production and immunoblotting

A synthetic peptide (CDITLQWLIDHSKAQR) corresponding to the C-terminus of ARL-8 conjugated with keyhole limpet hemocyanin was used to immunize rabbits. Antiserum was purified using the peptide-immobilized affinity column (Pierce). Worm protein extracts were prepared by heating adult worms in SDS-PAGE sample buffer (50 mM Tris-HCl (pH6.8), 10% (V/V) glycerol, 2% (W/V) SDS, 5% (V/V) β-mercaptoethanol, and 0.02% (W/V) Bromophenol blue) and subjected to 12% SDS-PAGE. Immunoblotting was performed as described previously (Kajiho et al., 2003).

Aldicarb Assay

Aldicarb sensitivity was examined by transferring young adult worms to plates containing 1 mM aldicarb and assaying the time course of paralysis as described previously (Mahoney et al., 2006). Locomotion was assessed every 20 minutes and animals were considered paralyzed if they appeared hypercontracted and failed to move even if prodded. For each experiment, 20–25 animals were tested and each experiment was repeated at least three times.

Dynamic imaging

Dynamic imaging was performed on an inverted Zeiss Axio Observer Z1 microscope equipped with a Plan-Apochromat 63×/1.4 objective and a QuantEM:512SC camera. All movies were acquired over 40 seconds with a speed of 7 frames per second and an exposure time of 100ms. Wild-type L4 worms were cultured at 25°C, while *arl-8(wy271)* animals were maintained at 20°C until the L3 stage and subsequently shifted to 25°C at the L3 stage to bypass embryonic and early larval lethality. For movie acquisition, worms were mounted onto 2% agarose pads and anesthetized with 6 mM levamisol for no longer than 20 minutes.

When necessary, movies were corrected for animal movement using the `register' plugin in ImageJ. Subsequently, axons were straightened with the plugin `straighten to line'. Finally, kymographs were constructed with the `kymograph' plugin. From these kymographs, vesicle speed, directionality and pause sites were deduced, with all data normalized by time and length of the imaged axonal segment.

To derive the average intensity of stable puncta, boxes were drawn around the vertical lines in the kymographs (which reflect stable puncta persisting throughout the movie) and the average intensity measured, minus any neighbouring background fluorescence. A similar procedure was performed for moving puncta. However, since these puncta are very small, a line instead of a box was drawn to calculate the average intensity after background subtraction. The probability that a moving puncta would stop upon encountering a stable one was calculated as follows. For each stable puncta, the number of transiting puncta and stopping puncta were measured from the kymographs, generating a probability dataset for various intensities of the stable puncta.

To obtain the disassociation rate, each punctum dissociating from a stable punctum was counted from kymographs. The sum of shed particles from one stable punctum was normalized to the movie acquisition time, yielding the disassociation rate per stable punctum.

Supplementary Material

Refer to Web version on PubMed Central for supplementary material.

Acknowledgments

This work was supported by the Howard Hughes Medical Institute, the Human Frontier Science Foundation and the W.M. Keck Foundation. We thank the International *C. elegans* Gene Knockout Consortium, the National Bioresource Project (Japan) and the labs of C. Bargmann, G. Lesa and Y. Jin for strains, D. Klopfenstein and S. Munro for reagents, and I. Kolotuev, Y. Schwab and M Labouesse for assistance with correlative EM. We also thank C. Gao and Y. Fu for technical assistance and S. Sigrist and S. Munro for thoughtful comments on the manuscript.

REFERENCES

Ahmari SE, Buchanan J, Smith SJ. Assembly of presynaptic active zones from cytoplasmic transport packets. Nat Neurosci. 2000; 3:445–451. [PubMed: 10769383]

Aikawa Y, Martin TF. ARF6 regulates a plasma membrane pool of phosphatidylinositol(4,5)bisphosphate required for regulated exocytosis. J Cell Biol. 2003; 162:647–659. [PubMed: 12925709]

Bagshaw RD, Callahan JW, Mahuran DJ. The Arf-family protein, Arl8b, is involved in the spatial distribution of lysosomes. Biochem Biophys Res Commun. 2006; 344:1186–1191. [PubMed: 16650381]

Bonanomi D, Benfenati F, Valtorta F. Protein sorting in the synaptic vesicle life cycle. Prog Neurobiol. 2006; 80:177–217. [PubMed: 17074429]

Bonifacino JS, Glick BS. The mechanisms of vesicle budding and fusion. Cell. 2004; 116:153–166. [PubMed: 14744428]

Brown HM, Van Epps HA, Goncharov A, Grant BD, Jin Y. The JIP3 scaffold protein UNC-16 regulates RAB-5 dependent membrane trafficking at C. elegans synapses. Dev Neurobiol. 2009; 69:174–190. [PubMed: 19105215]

Burre J, Volknandt W. The synaptic vesicle proteome. J Neurochem. 2007; 101:1448–1462. [PubMed: 17355250]

Cai H, Reinisch K, Ferro-Novick S. Coats, tethers, Rabs, and SNAREs work together to mediate the intracellular destination of a transport vesicle. Dev Cell. 2007; 12:671–682. [PubMed: 17488620]

Crump JG, Zhen M, Jin Y, Bargmann CI. The SAD-1 kinase regulates presynaptic vesicle clustering and axon termination. Neuron. 2001; 29:115–129. [PubMed: 11182085]

D'Souza-Schorey C, Chavrier P. ARF proteins: roles in membrane traffic and beyond. Nat Rev Mol Cell Biol. 2006; 7:347–358. [PubMed: 16633337]

Dai Y, Taru H, Deken SL, Grill B, Ackley B, Nonet ML, Jin Y. SYD-2 Liprin-alpha organizes presynaptic active zone formation through ELKS. Nat Neurosci. 2006; 9:1479–1487. [PubMed: 17115037]

Dai Z, Peng HB. Dynamics of synaptic vesicles in cultured spinal cord neurons in relationship to synaptogenesis. Mol Cell Neurosci. 1996; 7:443–452. [PubMed: 8875428]

Fergestad T, Davis WS, Broadie K. The stoned proteins regulate synaptic vesicle recycling in the presynaptic terminal. J Neurosci. 1999; 19:5847–5860. [PubMed: 10407025]

Fox RM, Von Stetina SE, Barlow SJ, Shaffer C, Olszewski KL, Moore JH, Dupuy D, Vidal M, Miller DM 3rd. A gene expression fingerprint of C. elegans embryonic motor neurons. BMC Genomics. 2005; 6:42. [PubMed: 15780142]

Gillingham AK, Munro S. The small G proteins of the Arf family and their regulators. Annu Rev Cell Dev Biol. 2007; 23:579–611. [PubMed: 17506703]

Graf ER, Daniels RW, Burgess RW, Schwarz TL, DiAntonio A. Rab3 dynamically controls protein composition at active zones. Neuron. 2009; 64:663–677. [PubMed: 20005823]

Hall DH, Hedgecock EM. Kinesin-related gene unc-104 is required for axonal transport of synaptic vesicles in C. elegans. Cell. 1991; 65:837–847. [PubMed: 1710172]

Hallam SJ, Jin Y. lin-14 regulates the timing of synaptic remodelling in Caenorhabditis elegans. Nature. 1998; 395:78–82. [PubMed: 9738501]

Harris TW, Hartwieg E, Horvitz HR, Jorgensen EM. Mutations in synaptojanin disrupt synaptic vesicle recycling. J Cell Biol. 2000; 150:589–600. [PubMed: 10931870]

Hermann GJ, Schroeder LK, Hieb CA, Kershner AM, Rabbitts BM, Fonarev P, Grant BD, Priess JR. Genetic analysis of lysosomal trafficking in Caenorhabditis elegans. Mol Biol Cell. 2005; 16:3273–3288. [PubMed: 15843430]

Hofmann I, Munro S. An N-terminally acetylated Arf-like GTPase is localised to lysosomes and affects their motility. J Cell Sci. 2006; 119:1494–1503. [PubMed: 16537643]

Hulett JM, Lueder F, Chan NC, Perry AJ, Wolynec P, Likic VA, Gooley PR, Lithgow T. The transmembrane segment of Tom20 is recognized by Mim1 for docking to the mitochondrial TOM complex. J Mol Biol. 2008; 376:694–704. [PubMed: 18187149]

Hunt-Newbury R, Viveiros R, Johnsen R, Mah A, Anastas D, Fang L, Halfnight E, Lee D, Lin J, Lorch A, et al. High-throughput in vivo analysis of gene expression in Caenorhabditis elegans. PLoS Biol. 2007; 5:e237. [PubMed: 17850180]

Jin Y, Garner CC. Molecular mechanisms of presynaptic differentiation. Annu Rev Cell Dev Biol. 2008; 24:237–262. [PubMed: 18588488]

Kajiho H, Saito K, Tsujita K, Kontani K, Araki Y, Kurosu H, Katada T. RIN3: a novel Rab5 GEF interacting with amphiphysin II involved in the early endocytic pathway. J Cell Sci. 2003; 116:4159–4168. [PubMed: 12972505]

Klassen MP, Shen K. Wnt signaling positions neuromuscular connectivity by inhibiting synapse formation in C. elegans. Cell. 2007; 130:704–716. [PubMed: 17719547]

Kolotuev I, Schwab Y, Labouesse M. A precise and rapid mapping protocol for correlative light and electron microscopy of small invertebrate organisms. Biol Cell. 102:121–132. [PubMed: 19807690]

Kostich M, Fire A, Fambrough DM. Identification and molecular-genetic characterization of a LAMP/CD68-like protein from Caenorhabditis elegans. J Cell Sci. 2000; 113(Pt 14):2595–2606. [PubMed: 10862717]

Kraszewski K, Mundigl O, Daniell L, Verderio C, Matteoli M, De Camilli P. Synaptic vesicle dynamics in living cultured hippocampal neurons visualized with CY3-conjugated antibodies directed against the lumenal domain of synaptotagmin. J Neurosci. 1995; 15:4328–4342. [PubMed: 7540672]

Krauss M, Kinuta M, Wenk MR, De Camilli P, Takei K, Haucke V. ARF6 stimulates clathrin/AP-2 recruitment to synaptic membranes by activating phosphatidylinositol phosphate kinase type Igamma. J Cell Biol. 2003; 162:113–124. [PubMed: 12847086]

Kreutzberg GW. Neuronal dynamics and axonal flow. IV. Blockage of intra-axonal enzyme transport by colchicine. Proc Natl Acad Sci U S A. 1969; 62:722–728. [PubMed: 4184255]

Mahoney TR, Liu Q, Itoh T, Luo S, Hadwiger G, Vincent R, Wang ZW, Fukuda M, Nonet ML. Regulation of synaptic transmission by RAB-3 and RAB-27 in Caenorhabditis elegans. Mol Biol Cell. 2006; 17:2617–2625. [PubMed: 16571673]

Margeta MA, Wang GJ, Shen K. Clathrin adaptor AP-1 complex excludes multiple postsynaptic receptors from axons in C. elegans. Proc Natl Acad Sci U S A. 2009; 106:1632–1637. [PubMed: 19164532]

Marza E, Long T, Saiardi A, Sumakovic M, Eimer S, Hall DH, Lesa GM. Polyunsaturated fatty acids influence synaptojanin localization to regulate synaptic vesicle recycling. Mol Biol Cell. 2008; 19:833–842. [PubMed: 18094048]

Matteoli M, Takei K, Perin MS, Sudhof TC, De Camilli P. Exoendocytotic recycling of synaptic vesicles in developing processes of cultured hippocampal neurons. J Cell Biol. 1992; 117:849–861. [PubMed: 1577861]

Miller KE, DeProto J, Kaufmann N, Patel BN, Duckworth A, Van Vactor D. Direct observation demonstrates that Liprin-alpha is required for trafficking of synaptic vesicles. Curr Biol. 2005; 15:684–689. [PubMed: 15823543]

Mullins C, Bonifacino JS. The molecular machinery for lysosome biogenesis. Bioessays. 2001; 23:333–343. [PubMed: 11268039]

Newell-Litwa K, Seong E, Burmeister M, Faundez V. Neuronal and nonneuronal functions of the AP-3 sorting machinery. J Cell Sci. 2007; 120:531–541. [PubMed: 17287392]

Nonet ML, Holgado AM, Brewer F, Serpe CJ, Norbeck BA, Holleran J, Wei L, Hartwieg E, Jorgensen EM, Alfonso A. UNC-11, a Caenorhabditis elegans AP180 homologue, regulates the size and protein composition of synaptic vesicles. Mol Biol Cell. 1999; 10:2343–2360. [PubMed: 10397769]

Nonet ML, Staunton JE, Kilgard MP, Fergestad T, Hartwieg E, Horvitz HR, Jorgensen EM, Meyer BJ. Caenorhabditis elegans rab-3 mutant synapses exhibit impaired function and are partially depleted of vesicles. J Neurosci. 1997; 17:8061–8073. [PubMed: 9334382]

Okada Y, Yamazaki H, Sekine-Aizawa Y, Hirokawa N. The neuron-specific kinesin superfamily protein KIF1A is a unique monomeric motor for anterograde axonal transport of synaptic vesicle precursors. Cell. 1995; 81:769–780. [PubMed: 7539720]

Okai T, Araki Y, Tada M, Tateno T, Kontani K, Katada T. Novel small GTPase subfamily capable of associating with tubulin is required for chromosome segregation. J Cell Sci. 2004; 117:4705–4715. [PubMed: 15331635]

Owald D, Sigrist SJ. Assembling the presynaptic active zone. Curr Opin Neurobiol. 2009; 19:311–318. [PubMed: 19395253]

Pack-Chung E, Kurshan PT, Dickman DK, Schwarz TL. A Drosophila kinesin required for synaptic bouton formation and synaptic vesicle transport. Nat Neurosci. 2007; 10:980–989. [PubMed: 17643120]

Paduch M, Jelen F, Otlewski J. Structure of small G proteins and their regulators. Acta Biochim Pol. 2001; 48:829–850. [PubMed: 11995995]

Pasqualato S, Renault L, Cherfils J. Arf, Arl, Arp and Sar proteins: a family of GTP-binding proteins with a structural device for 'front-back' communication. EMBO Rep. 2002; 3:1035–1041. [PubMed: 12429613]

Patel MR, Lehrman EK, Poon VY, Crump JG, Zhen M, Bargmann CI, Shen K. Hierarchical assembly of presynaptic components in defined C. elegans synapses. Nat Neurosci. 2006; 9:1488–1498. [PubMed: 17115039]

Poon VY, Klassen MP, Shen K. UNC-6/netrin and its receptor UNC-5 locally exclude presynaptic components from dendrites. Nature. 2008; 455:669–673. [PubMed: 18776887]

Schluter OM, Schmitz F, Jahn R, Rosenmund C, Sudhof TC. A complete genetic analysis of neuronal Rab3 function. J Neurosci. 2004; 24:6629–6637. [PubMed: 15269275]

Schuske KR, Richmond JE, Matthies DS, Davis WS, Runz S, Rube DA, van der Bliek AM, Jorgensen EM. Endophilin is required for synaptic vesicle endocytosis by localizing synaptojanin. Neuron. 2003; 40:749–762. [PubMed: 14622579]

Shapira M, Zhai RG, Dresbach T, Bresler T, Torres VI, Gundelfinger ED, Ziv NE, Garner CC. Unitary assembly of presynaptic active zones from Piccolo-Bassoon transport vesicles. Neuron. 2003; 38:237–252. [PubMed: 12718858]

Sieburth D, Ch'ng Q, Dybbs M, Tavazoie M, Kennedy S, Wang D, Dupuy D, Rual JF, Hill DE, Vidal M, et al. Systematic analysis of genes required for synapse structure and function. Nature. 2005; 436:510–517. [PubMed: 16049479]

Takamori S, Holt M, Stenius K, Lemke EA, Gronborg M, Riedel D, Urlaub H, Schenck S, Brugger B, Ringler P, et al. Molecular anatomy of a trafficking organelle. Cell. 2006; 127:831–846. [PubMed: 17110340]

Tao-Cheng JH. Ultrastructural localization of active zone and synaptic vesicle proteins in a preassembled multi-vesicle transport aggregate. Neuroscience. 2007; 150:575–584. [PubMed: 17977664]

Treusch S, Knuth S, Slaugenhaupt SA, Goldin E, Grant BD, Fares H. Caenorhabditis elegans functional orthologue of human protein h-mucolipin-1 is required for lysosome biogenesis. Proc Natl Acad Sci U S A. 2004; 101:4483–4488. [PubMed: 15070744]

Tsukita S, Ishikawa H. The movement of membranous organelles in axons. Electron microscopic identification of anterogradely and retrogradely transported organelles. J Cell Biol. 1980; 84:513–530. [PubMed: 6153657]

White JG, Southgate E, Thomson JN, Brenner S. The structure of the ventral nerve cord of Caenorhabditis elegans. Philos Trans R Soc Lond B Biol Sci. 1976; 275:327–348. [PubMed: 8806]

Zhai RG, Vardinon-Friedman H, Cases-Langhoff C, Becker B, Gundelfinger ED, Ziv NE, Garner CC. Assembling the presynaptic active zone: a characterization of an active one precursor vesicle. Neuron. 2001; 29:131–143. [PubMed: 11182086]

Zhang B, Koh YH, Beckstead RB, Budnik V, Ganetzky B, Bellen HJ. Synaptic vesicle size and number are regulated by a clathrin adaptor protein required for endocytosis. Neuron. 1998; 21:1465–1475. [PubMed: 9883738]

Zhen M, Jin Y. The liprin protein SYD-2 regulates the differentiation of presynaptic termini in C. elegans. Nature. 1999; 401:371–375. [PubMed: 10517634]

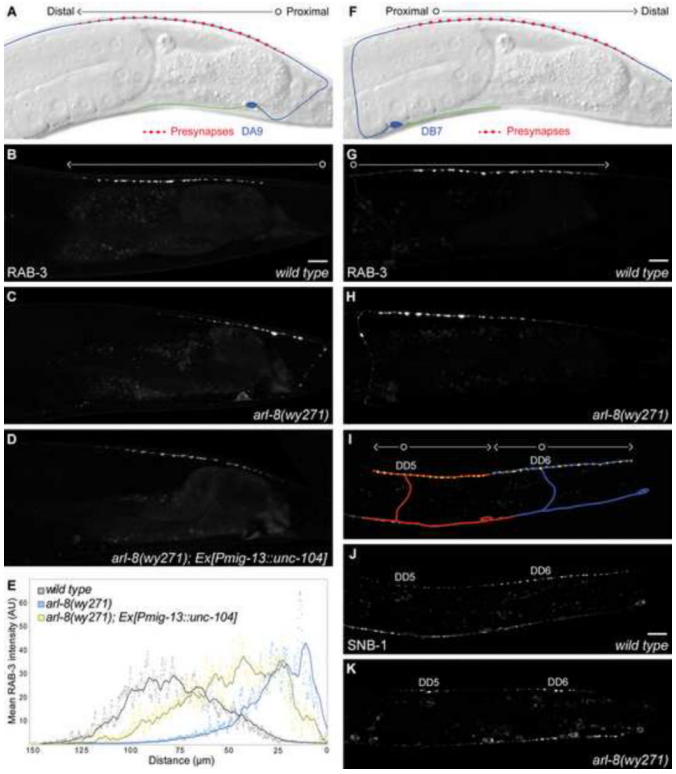

Figure 1. *wy271* Mutants Display Abnormal Proximodistal Targeting of Synaptic Vesicle Proteins

(A) Diagram representing wild-type morphology and presynaptic patterning in DA9. Proximodistal polarity is represented by an open circle (proximal) transitioning to an arrowhead (distal). Fluorescence of the gut and anus is occasionally visible. (B–D) Targeting of the SV-associated protein GFP::RAB-3 in adult *wild type* (B), *arl-8(wy271)* (C) and *wyEx2694[Pmig-13::unc-104]; arl-8(wy271)* (D) DA9 neurons. *wyIs85*. (E) Mean GFP::RAB-3 intensity of 20 DA9 dorsal axons as a function of distance from the DA9 commissure. Dots represent single pixel averages across the y-axis while the lines reflect 10 μm moving averages of these values. (F) Diagram representing wild-type morphology and presynaptic patterning in DB7. (G, H) Targeting of GFP::RAB-3 in *wild type* (G) and *arl-8(wy271)* (H) DB7 neurons. *wyEx1199*. (I) Diagram representing wild-type morphology and presynaptic patterning in DD5 and DD6. Proximodistal extension in DD neurons reflects a bifurcation of the dorsal axon, with proximal defined by the location of the branch point and labelled with the corresponding DD name. (J, K) Targeting of the integral SV protein SNB-1::GFP in *wild type* and *arl-8(wy271)* DD neurons at the L3 developmental stage. *juIs1*. Scale bars, 10 μm. See also Figure S1.

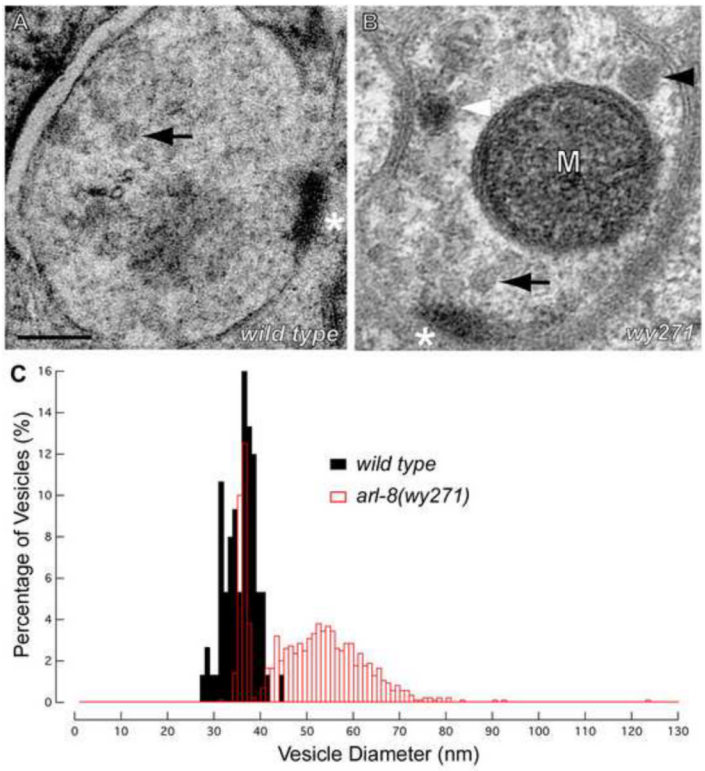

Figure 2. Synaptic Vesicles Ectopically Accumulate in the Proximal Axon in *wy271* Mutants

(A–B) Electron micrographs of a wild-type presynapse (A) and a proximal ectopic RAB-3 accumulation in *arl-8(wy271)* mutant animals (B). Arrows, standard-size clear core synaptic vesicles. Black arrowhead, large-diameter clear core vesicle. White arrowhead, dense core vesicle. M, mitochondrion. Asterisk, active zone structures. Scale bar, 100 nm. (C) Distribution of synaptic vesicle diameter in *wild type* and *arl-8(wy271)* mutant animals. n=75 for *wild type*. n=838 for *arl-8(wy271)*. See also Figure S2.

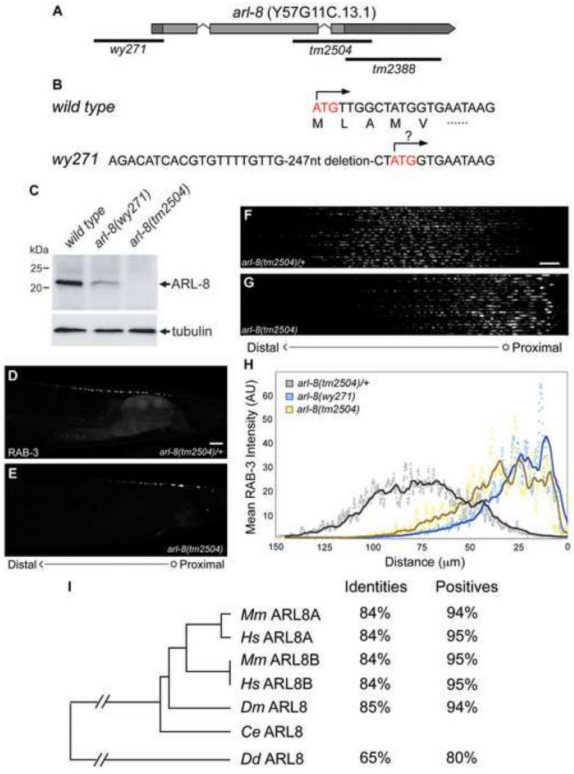

Figure 3. *wy271* Represents a Strong Hypomorphic Lesion in the Conserved Arf-like Small G protein *arl-8*

(A,B) Genomic architecture of the *arl-8* locus, with corresponding genetic lesions. (C) Western blot analysis of *wild type*, *arl-8(wy271)* and *arl-8(tm2504)* worm lysates using a polyclonal antibody against ARL-8. Note: Because the antibody was raised against a C-terminal peptide that is deleted in the *tm2504* allele, the absence of staining in this allele likely reflects the loss of the epitope and confirms the specificity of the antibody. (D–E) Targeting of GFP::RAB-3 in DA9 neurons in *arl-8(tm2504)/+* heterozygous control animals (D) and *arl-8(tm2504)* homozygous progeny from heterozygous mothers (E). *wyIs85*. Note: *arl-8(tm2504)* is maternal lethal and kept as a balanced heterozygous strain. (F–G) Confocal micrographs of 20 *arl-8(tm2504)/+* (F) and *arl-8(tm2504)* (G) DA9 dorsal axons, straightened and aligned along their anteroposterior axis. (H) Mean GFP::RAB-3 intensity of 20 DA9 dorsal axons as a function of distance from the DA9 commissure. Dots represent single pixel averages across the y-axis while the lines reflect 10 μm moving averages of these values. The data for *arl-8(wy271)* are the same as shown in Figure 1E and presented here for comparison with *arl-8(tm2504)*. (I) Phylogenetic tree and sequence identity and similarity among putative *arl-8* orthologs. Ce, Caenorhabditis elegans; Dd, Dictyostelium discoideum; Dm, Drosophila melanogaster; Hm, Homo sapiens; Mm, Mus musculus. See also Figures S3 and S4.

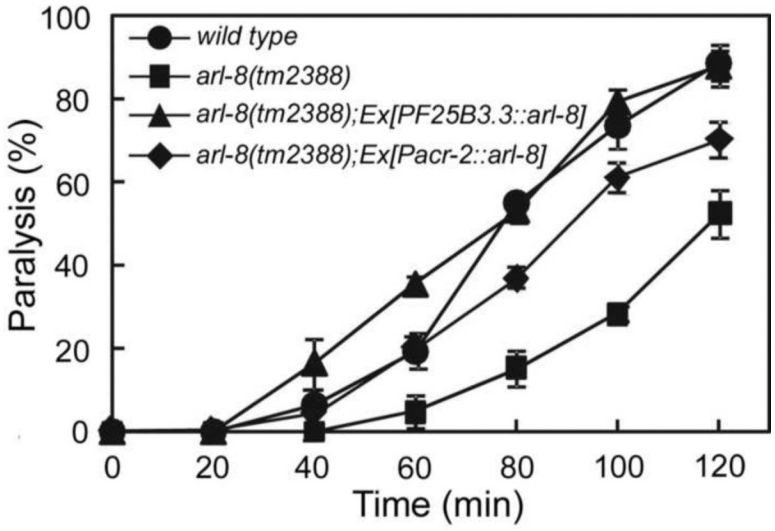

Figure 4. Aldicarb Resistance of *arl-8(tm2388)* Mutants

Time course of paralysis for wild type, arl-8(tm2388), arl-8(tm2388);Ex[Pacr-2::arl-8] (tdEx564) and *arl-8(tm2388);Ex[PF25B3.3::arl-8] (tdEx655*) animals in the presence of aldicarb. Error bars, SEM.

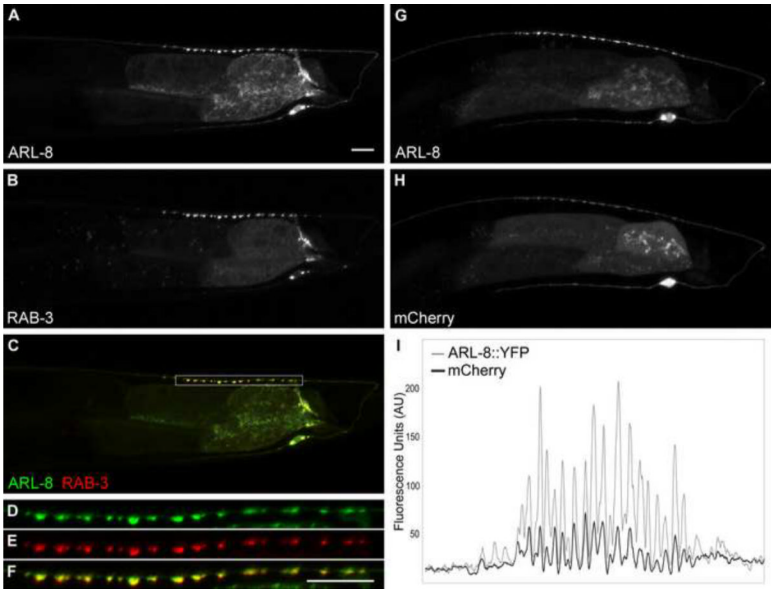

Figure 5. ARL-8::YFP is Strongly Enriched at the Presynaptic Terminal

(A–F) Colocalization of ARL-8::YFP (A, D) with mCherry::RAB-3 (B,E), double label (C,F), high magnification (D–F) in DA9. *wyEx3198.* (G–I) Enrichment of ARL-8::YFP (G) over cytosolic mCherry (H), quantified by a 1.4 μm moving average line scan (I). *wyEx3235*. Scale bars, 10 μm.

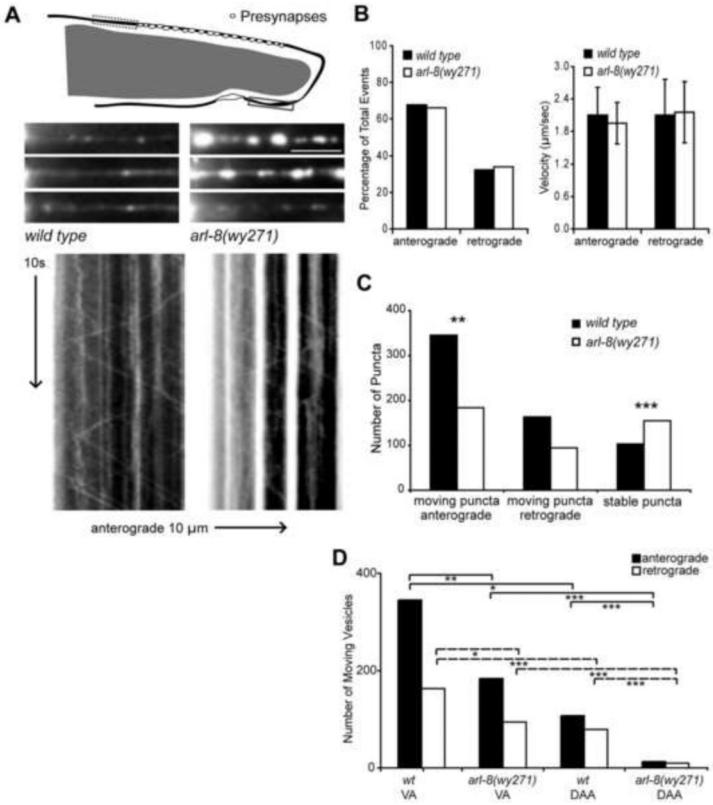

Figure 6. Dynamic Imaging Suggests a Selective Deficit in Maintaining the Trafficking State in *arl-8* Mutants

(A) Diagram and representative images of the ventral axon initial segment imaging area (VA, solid-line box) and kymographs generated using a high-sensitivity CCD camera. *wyEx2793*. Scale bar, 10 µm. (B) Graphs representing the percentage of anterograde and retrograde trafficking events (left) and the velocity of GFP::RAB-3 trafficking (right) in the ventral axon. Left, t test, n=278–508 moving particles; Right, Error Bars, SEM, t test, n=94–345 moving particles. (C) Graph representing the incidence of moving particles and stable particles in the ventral axon. **p<0.01, ***p<0.0001, t test, n=103–341 particles. (D) Graph comparing the number of anterograde and retrograde moving particles in the distal asynaptic axon (DAA, dashed-line box in (A)) and ventral axon (VA). *p<0.05, **p<0.005, ***p<0.0005, t test, n=10–345 moving particles. See also Figures S5, S6 and S7.

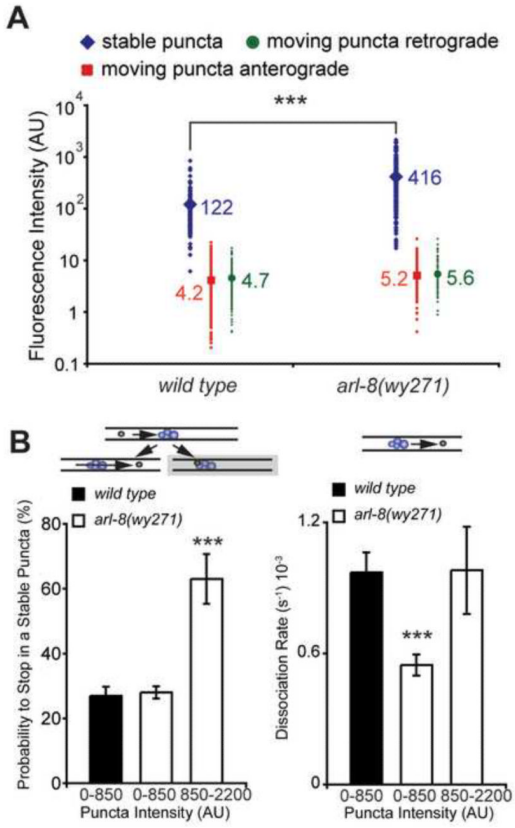

Figure 7. Synaptic Vesicle Precursors Exhibit an Enhanced Tendency to Aggregate in *arl-8* Mutants

(A) Quantification of the mean intensity of moving and stable particles. n=103–341 particles. (B) Left: Graph representing the probability that a moving particle will stall upon encountering a stable particle of a given GFP::RAB-3 intensity during the imaging session. n=24–177 stable particles. Right: Graph representing the rate that a stable punctum gives rise to a mobile punctum. n=27–193 stable particles. Statistics for all panels are t test with *** $p<0.0001$. Error bars, SEM. See also Figure S8.

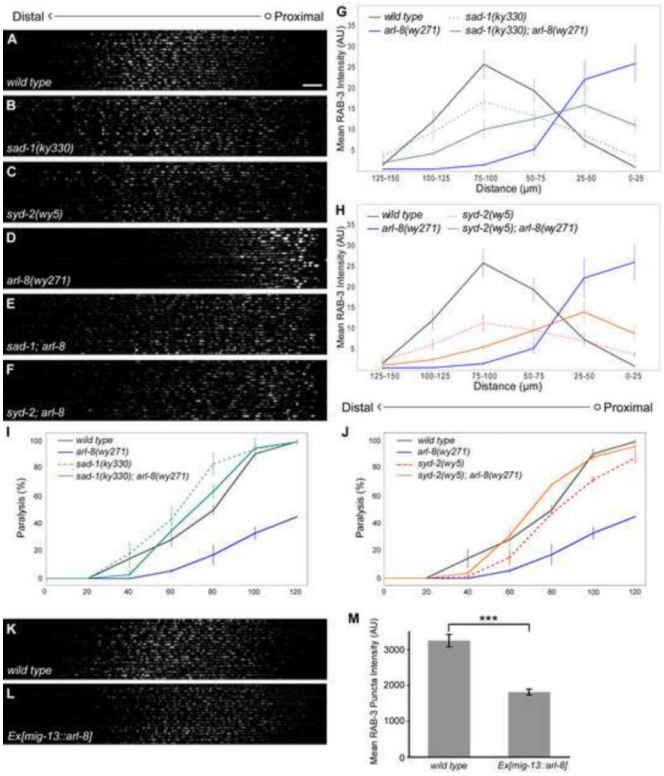

Figure 8. The Premature Accumulation of Presynaptic Cargoes in *arl-8* Mutants is Strongly Dependent Upon Known Positive Regulators of Presynaptic Assembly

(A–F) Confocal micrographs of 20 *wild type* (A), *sad-1(ky330)* (B), *syd-2(wy5)* (C), *arl-8(wy271)* (D), *sad-1(ky330); arl-8(wy271)* (E) and *syd-2(wy5); arl-8(wy271)* (F) DA9 dorsal axons, straightened and aligned along their anteroposterior axis. Scale bar, 10 μm. (G–H) Quantification of mean GFP::RAB-3 distribution along the DA9 dorsal axon, binned into 25 μm segments for statistical purposes. n=20 animals. (I–J) Time course of paralysis for wild type, sad-1(ky330), syd-2(wy5), arl-8(wy271), sad-1(ky330); arl-8(wy271) and *syd-2(wy5); arl-8(wy271)* animals in the presence of aldicarb. (K–L) Confocal micrographs of 20 *wild type* (K) and *arl-8* overexpressing (L) animals (*wyEx3668* and *wyIs85*). (M) Quantification of mean RAB-3 puncta fluorescence intensity. n=550–576 puncta. Statistics for all panels are t test with *** $p<0.0001$. Error bars, SEM.